ICANS XIV
14th Meeting of the International Collaboration on
Advanced Neutron Sources
June 14-19, 1998
Starved Rock Lodge, Utica, IL

DESIGN AND PLACEMENT CONSIDERATIONS FOR PROPELLER-TYPE T-ZERO CHOPPERS

R. A. Robinson, Los Alamos National Laboratory, Los Alamos, NM 87545

We discuss factors to do with placement and running speeds of "propeller-type" t-zero choppers, as implemented at ISIS (on chopper spectrometers) and at LANSCE (on a reflectometer, chopper spectrometer and small-angle scattering instrument).

Propeller-syle t-zero choppers have been used at spallation sources since the HET chopper spectrometer was originally constructed[1], and similar t-zero choppers have been installed on other chopper instruments[2] at ISIS, as well as on the SPEAR reflectometer, the PHAROS chopper spectrometer[3] and, more recently, the LQD small-angle machine at LANSCE. In all cases, the purpose is to block the burst of high-energy neutrons that emanates from the source when the proton beam strikes the target, and still be fully open when the thermal neutrons of interest pass through the space occupied by the t-zero chopper. In general, roughly 30 cm of high-strength high-Ni alloy (like nimonic or inconel) is placed in the beam, and for background purposes, it is desirable to place the chopper as far upstream as possible. Examples of rotor geometries are shown in Fig. 1, while Fig. 2 is a photograph of the 341 kg inconel rotor used in the PHAROS t-zero chopper.

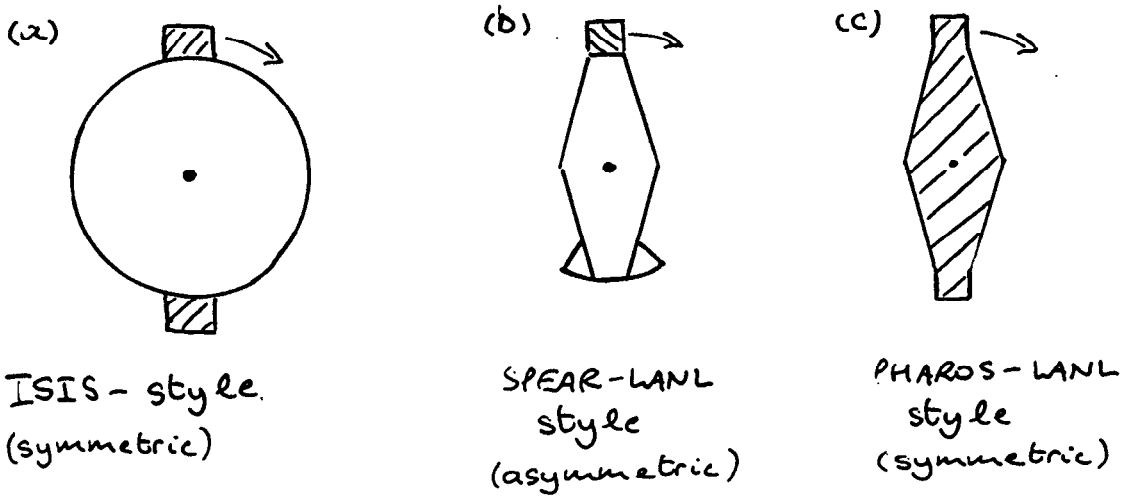

Figure 1 Schematic diagram showing t-zero choppers as implemented (a) at ISIS, (b) on SPEAR and LQD at LANSCE, and (c) on PHAROS at LANSCE. The neutron-attenuating material is shown by the shading and an alumunium alloy is typically used for the other structural components. (a) and (c) are *symmetrically* balanced, with the rotor entering the beam twice per revolution, while (b) is *asymmetrically* balanced and enters only once per revolution.

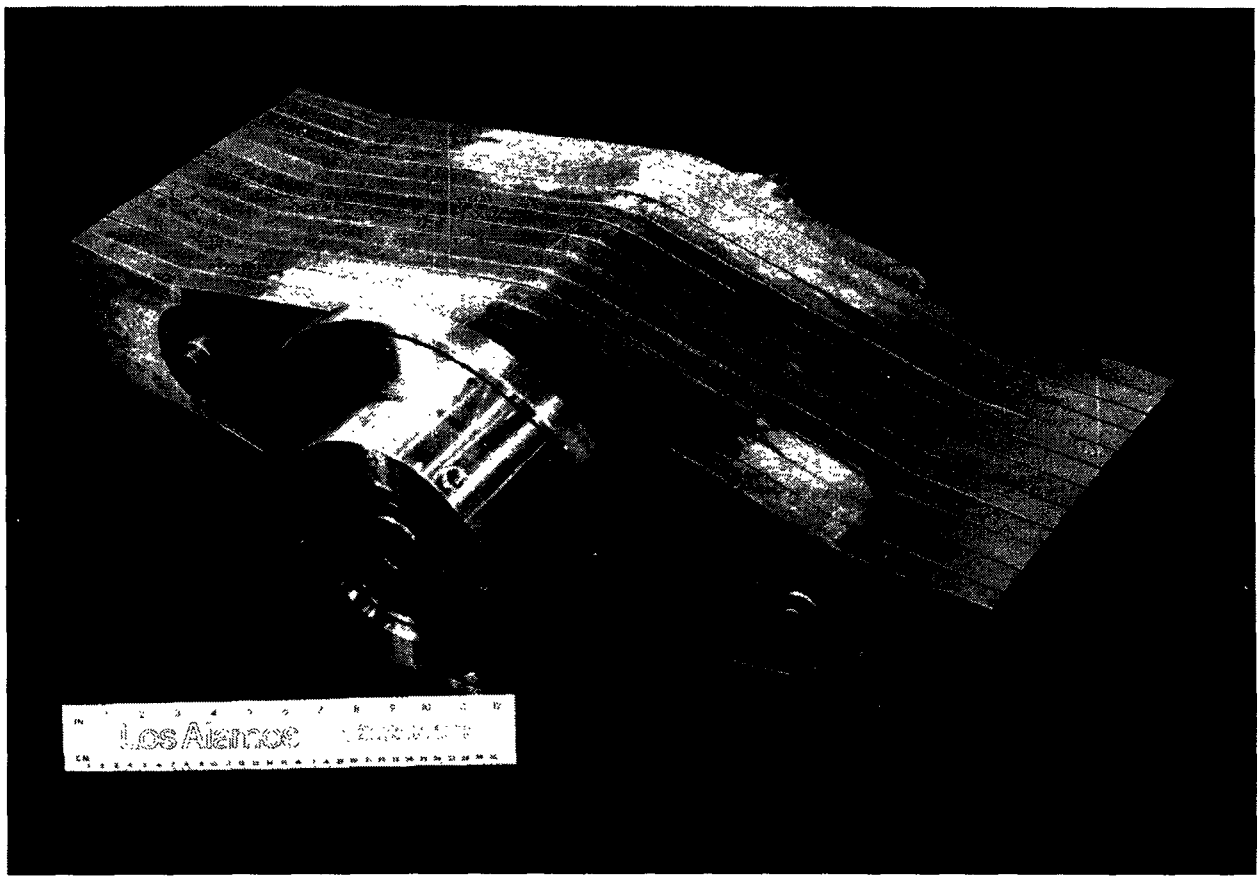

Figure 2 Photograph of the rotor for the t-zero chopper on the high-resolution chopper spectrometer PHAROS (see Ref. 3) at LANSCE. The rotor is symmetrically balanced, and the neutron beam passes throught the square sections at the ends of the blades. It is constructed from a set of twelve 25-mm thick plates of Inconel X-750, and weighs 341 kg.

Table I lists those parameters that are available to perform an optimisation, along with constraints, typical outer bounds and the values actually used on the high-resolution chopper spectrometer PHAROS[3] at LANSCE. As regards materials, we use Inconel X-750 [4], a high-tensile-strength high-nickel alloy (density ρ = 8.3 g cm^{-3}; yield strength σ_{yield} = 690 MPa; fast-neutron mean free path = 3.4 cm) as the neutronic element in our t-zero choppers. Following practice at ISIS, we have used 30 cm of inconel (as measured along the neutron beam path), which corresponds to ~ 8.8 fast-neutron mean free paths. The next constraint to consider is the maximum rotational frequency ν_{max} at which such a chopper can be run, without disintegrating. For a rotating straight homogeneous bar, with width « length, ν_{max} is given by

$$\nu_{max} = \frac{1}{2\pi}\sqrt{\frac{2\sigma_{yield}}{\rho R^2}} \qquad (1),$$

where σ_{yield} is the yield stress for the bar material, ρ is its density, R is the overall radius of the rotor and the maximum stress is at the centre of rotation. Assuming an additional engineering safety factor S (which should typically be ~3), the equation becomes

$$\nu_{max} = \frac{1}{2\pi}\sqrt{\frac{2\sigma_{yield}}{S\rho R^2}} \qquad (2).$$

and this limit is shown as a function of R in Fig. 3.

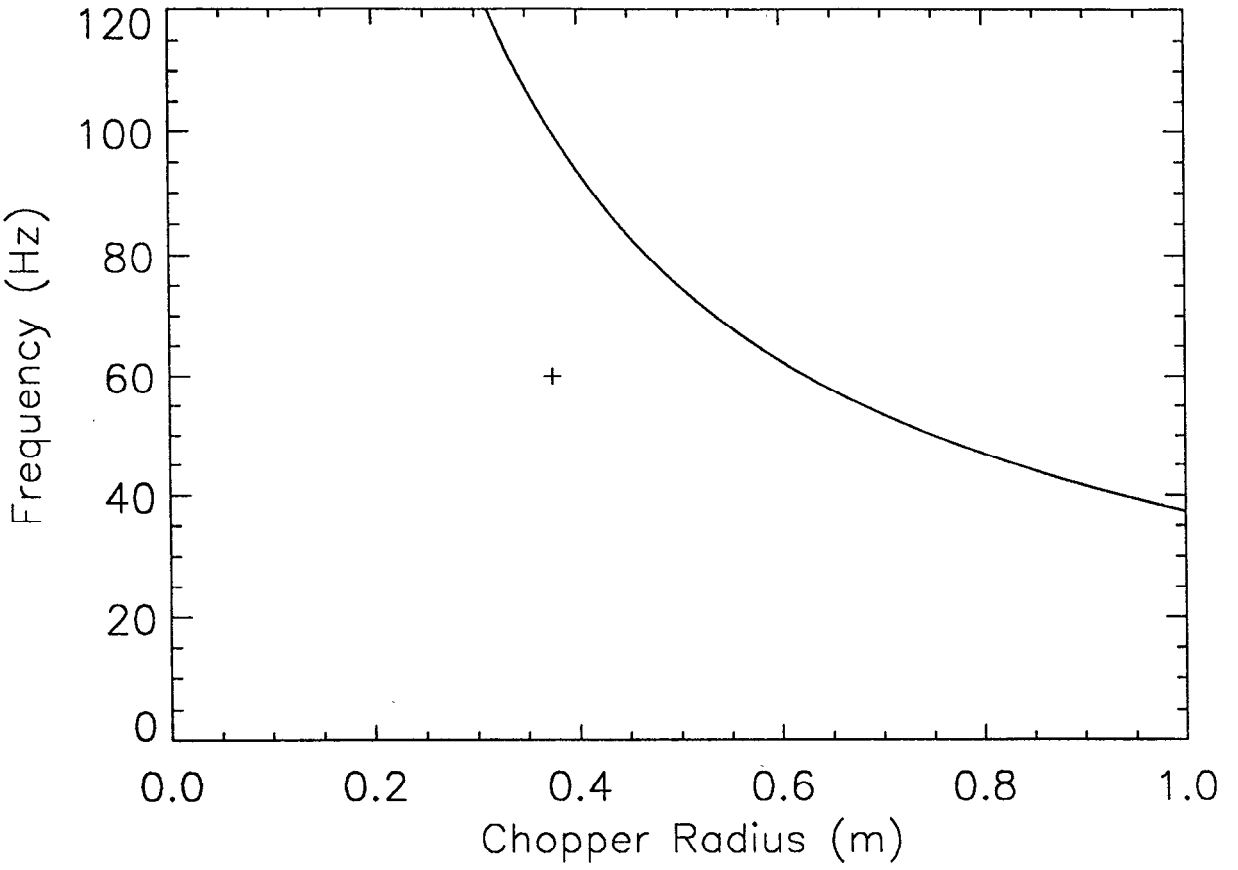

Figure 3 Chopper frequency - radius bounds determined from the yield stress and density of Inconel X-750, using Equation (2) with an engineering safety factor S = 3. In designing the chopper, one must remain on the lower left-hand side of the line. The (+) symbol represents the rotor used on PHAROS.

The next consideration is the spatial extent of the neutron beam, at the chopper location. Normal thermal beams are defined by a series of thermal-neutron apertures, typically sintered B_4C or a low-epoxy/B_4C composite (crispy-mix). Between these apertures, but with larger width, there is likely some fast-neutron shielding, typically consisting of some combination of steel and a hydrogenous material (e.g. polyethylene or epoxy resin, possibly doped with borax), as shown in Fig. 4(a). It is advantageous to think of a *thermal-neutron* beam and a larger *fast-neutron* beam coexisting at the chopper position. Similar ideas apply to beams with guides, as shown in Fig. 4(b), but it is not so clear in this case what the shape and extent of the fast-neutron beam is. In both cases, it is clearly desirable to sweep the chopper blade across the shortest dimension of the beam, and this may have consequences regarding whether the rotation axis of the rotor is below (or above) the neutron beam or is translated to one side. **The main function of the t-zero chopper is to block the fast neutron beam as fully as possible, when protons strike the**

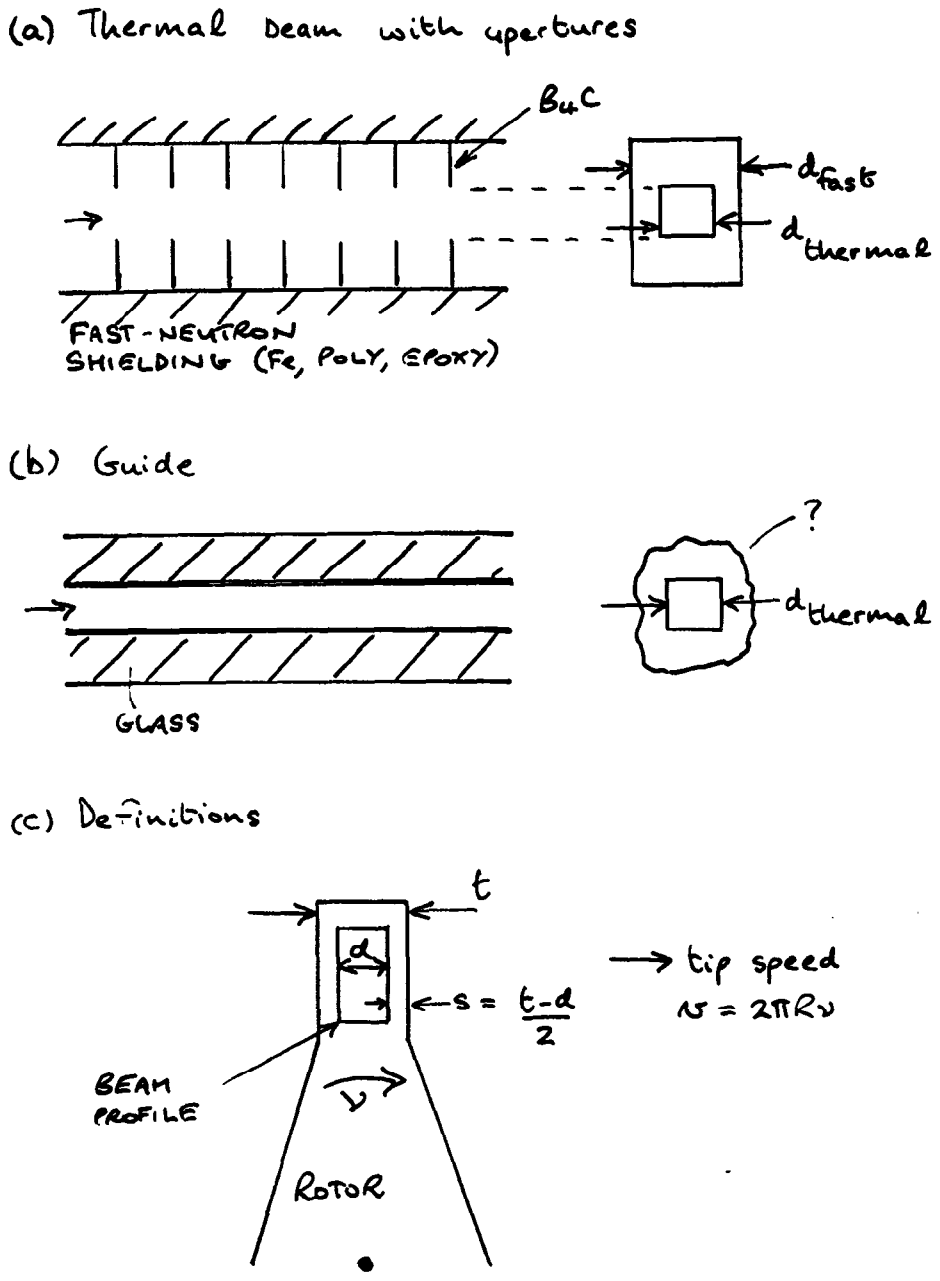

Figure 4 Schematic diagram showing the thermal and fast-neutron beams for (a) a normal thermal beam using apertures (B_4C) and larger aperture fast-neutron shielding (steel, polyethylene, epoxy resin), and (b) for a guide, in which the fast-neutron aperture is less well-defined. In (a) and (c), some of the symbols used in the text for chopper and beam dimensions are shown.

spallation target, and yet have the thermal beam fully open in time for the highest energy neutrons of interest to pass through completely unimpeded. The latter condition is not so straightforward, and the ISIS t-zero choppers on HET and MARI are not fully open at 1eV, for instance. If one simply considers a fixed point on the chopper sweeping across the thermal beam of width $d_{thermal}$, the maximum neutron energy E_{max} that can pass through is

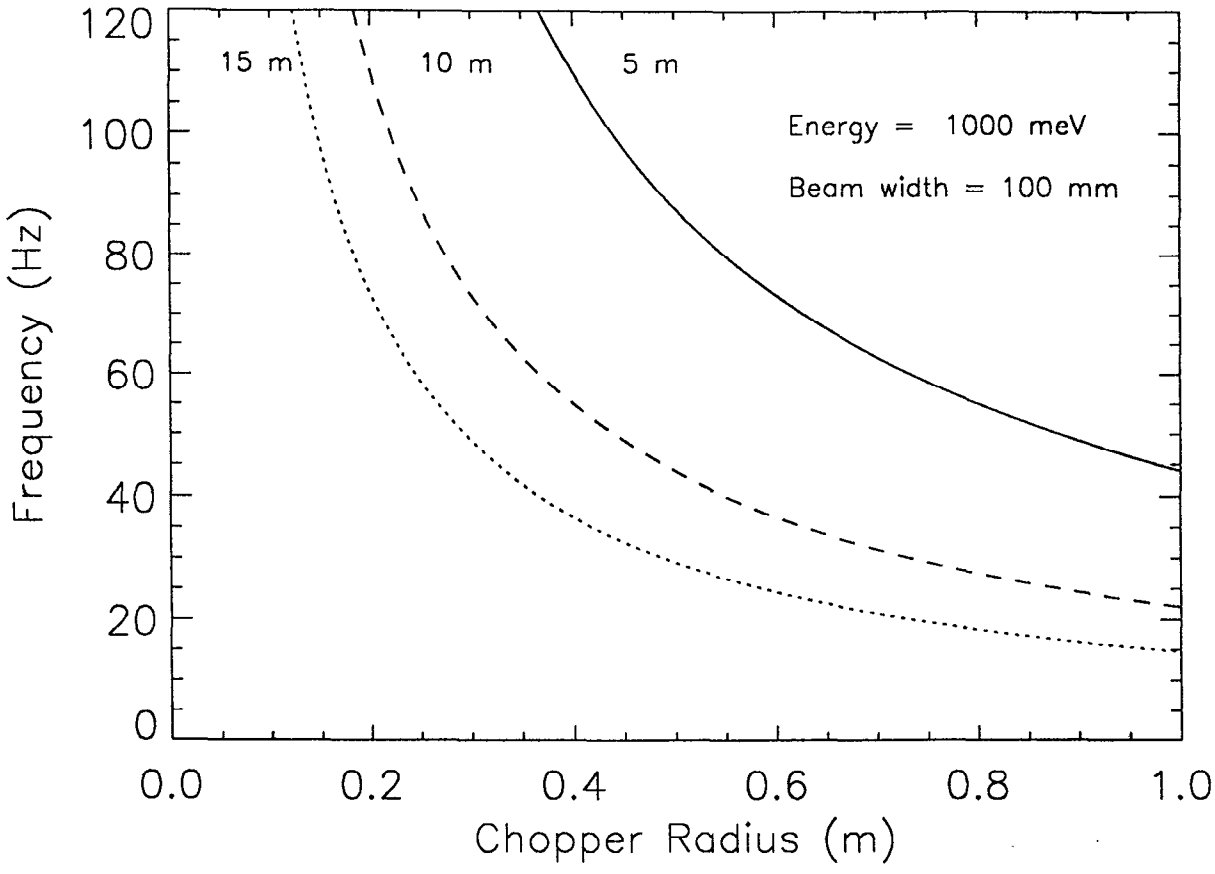

Figure 5 Chopper frequency - radius bounds determined from the desired maximum useful neutron energy E_{max}, beam width $d_{thermal}$ and for source-chopper distance = 5, 10 and 15 m, using Equation (3). For the example shown here, we assume E_{max} = 1 eV and $d_{thermal}$ = 10 cm. The chopper must operate in the region to the upper right-hand side of the curve.

$$E_{max}(meV) = 5.22697 \times 10^{-6} \left(\frac{2\pi\nu RL}{d_{thermal}} \right)^2 \qquad (3).$$

The parameters that are available to the instrument designer, for a given desired E_{max} and beam width $d_{thermal}$, are the chopper rotational frequency ν, the chopper radius R and the distance L at which chopper is placed, measured from the source. As an example, Fig. 5 shows a set of frequency-radius curves for different chopper placements, assuming a 10-cm wide beam and the use of neutrons up to 1eV. One needs to be to the upper-right side of these lines, and it is very difficult to achieve this, by placing the chopper at the edge of the biological shield (say at 5m) - it involves either a very large or a very fast rotor. Equations (2) and (3) can now be combined into a very useful rule of thumb for chopper design, because they both have the same $\nu = 1/R$ functional dependence:

$$\frac{d_{thermal}}{2\pi L} \sqrt{\frac{E_{max}(meV)}{5.22697 \times 10^{-6}}} < R\nu < \frac{1}{2\pi} \sqrt{\frac{2\sigma_{yield}}{S\rho}} \qquad (4),$$

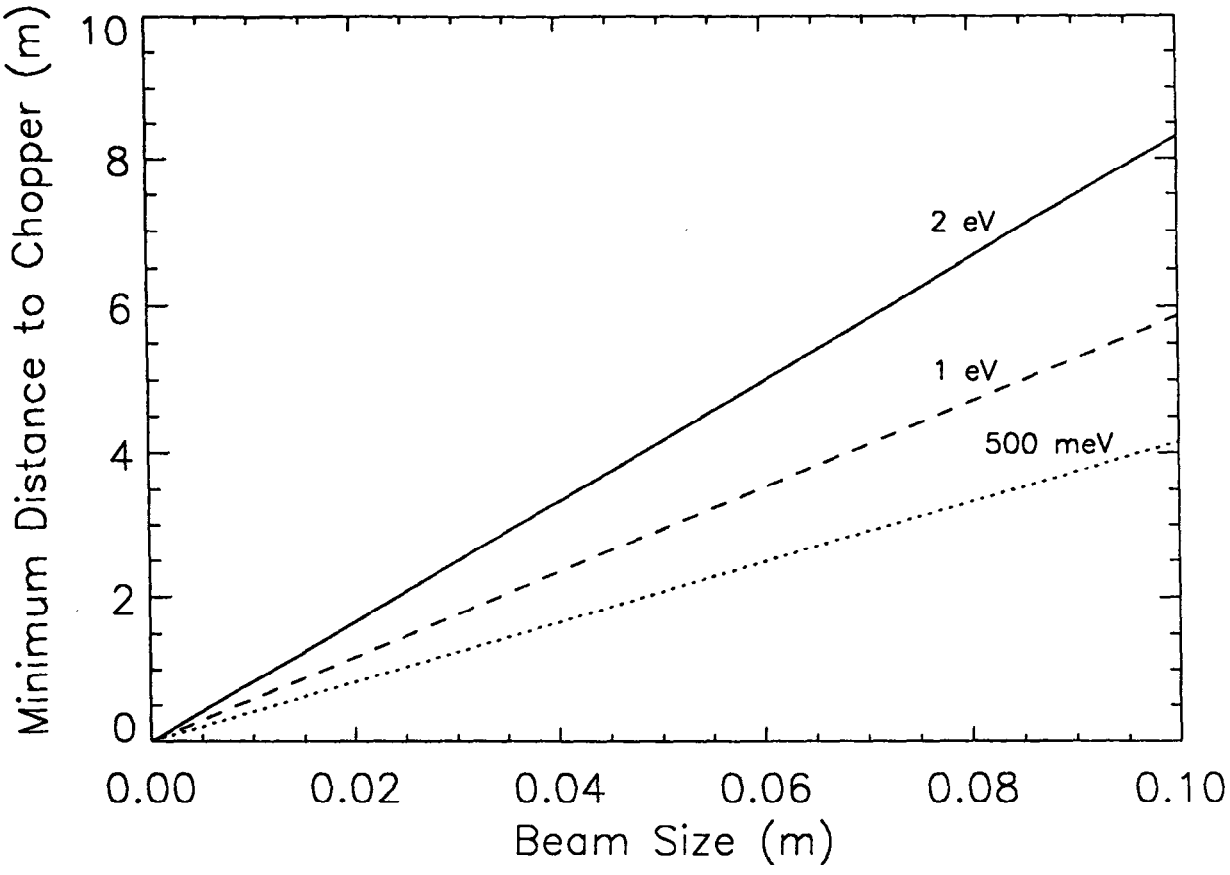

Figure 6 Plot of closest possible chopper position versus beam size for several neutron energies, following Equation (5). The numbers presented here, which assume the use of Inconel X-750 and a safety factor S = 3, take no account of the overlap of the chopper, beyond the beam size. This effect can be included simply by using s + d in place of d for the beam size in Equation (5).

or stated another way that is independent of R and ν,

$$L > d_{thermal}\sqrt{\frac{E_{max}(meV)}{5.22697\times10^{-6}}\frac{S\rho}{2\sigma_{yield}}} \qquad (5).$$

This linear L-versus-d variation is plotted in Fig. 6 for several neutron energies. Note that this expression is independent of both chopper radius R and chopper frequency ν, with the consequence that there are minimum acceptable source-chopper distances, irrespective of how one changes R and ν.

Now, Equation (3) and Fig. 5 correspond to the situation of having a chopper blade with width exactly equal to the beam size, with no overlap. In other words, it may not stop the whole fast-neutron beam which can proceed into the instrument and cause background problems, nor does it allow any margin for error in synchronising the chopper with the source. It is clearly desirable to make the chopper blade somewhat wider (say, with width t) as shown in Fig. 4(c), and one can

then define neutron energies at which the thermal beam starts to open (E_{start}) and at which it is fully open (E_{full}):

$$E_{start} = 5.22697\times10^{-6}\left(\frac{2\pi\nu RL}{s_{thermal}}\right)^2 \qquad (6)$$

$$= 5.22697\times10^{-6}\left(\frac{4\pi\nu RL}{t - d_{thermal}}\right)^2$$

and

$$E_{full} = 5.22697\times10^{-6}\left(\frac{2\pi\nu RL}{s_{thermal} + d_{thermal}}\right)^2 \qquad (7),$$

$$= 5.22697\times10^{-6}\left(\frac{4\pi\nu RL}{t + d_{thermal}}\right)^2$$

where s is the degree of overlap on the trailing edge of the chopper blade, and the second line of each equation assumes that the chopper blade is centred on the neutron beam when protons hit the target. **Equation 7 is particularly useful for determining how much overlap one can tolerate, given a desired value of E_{full}.** Of course, for the fast-neutron beam, there are corresponding equations in which $s_{thermal}$ and $d_{thermal}$ are replaced by s_{fast} and d_{fast}.

The overlap s_{fast} (see Fig. 4(c)) also determines how well the chopper and accelerator must be phased to each other, or how much jitter is acceptable in the chopper-accelerator timing-control system:

$$t_{jitter}(\mu s) = \frac{10^6 s_{fast}}{2\pi\nu R} = \frac{10^6 (t - d_{fast})}{4\pi\nu R} \qquad (8)$$

and one can replace s_{fast} and d_{fast} by $s_{thermal}$ and $d_{thermal}$ to give the equivalent fast-neutron jitter.

One also has to choose whether to construct the chopper such that it is *symmetrically* balanced, with the rotor entering the beam every 180°, or *asymmetrically* balanced in such a way that the rotor only re-enters the beam after a full revolution, as shown in Fig. 1(b). This effect is shown schematically in Fig. 7(a), for the PHAROS t-zero chopper parameters, in the time domain. Symmetric choppers are generally undesirable for broad-band cold-neutron applications, because the rotor re-enters the beam at a time corresponding to useful neutron bandwidth, and the uninterrupted wavelength bandwidth can be doubled using an asymmetric rotor - such choppers are used on SPEAR and LQD at LANSCE. However, asymmetric rotors can be more complicated to fabricate and balance. The energies at which the rotor re-enters the beam are

$$E_{180}(meV) = 5.22697\times10^{-6}\left(\frac{2L}{\nu}\right)^2 \qquad (9)$$

and

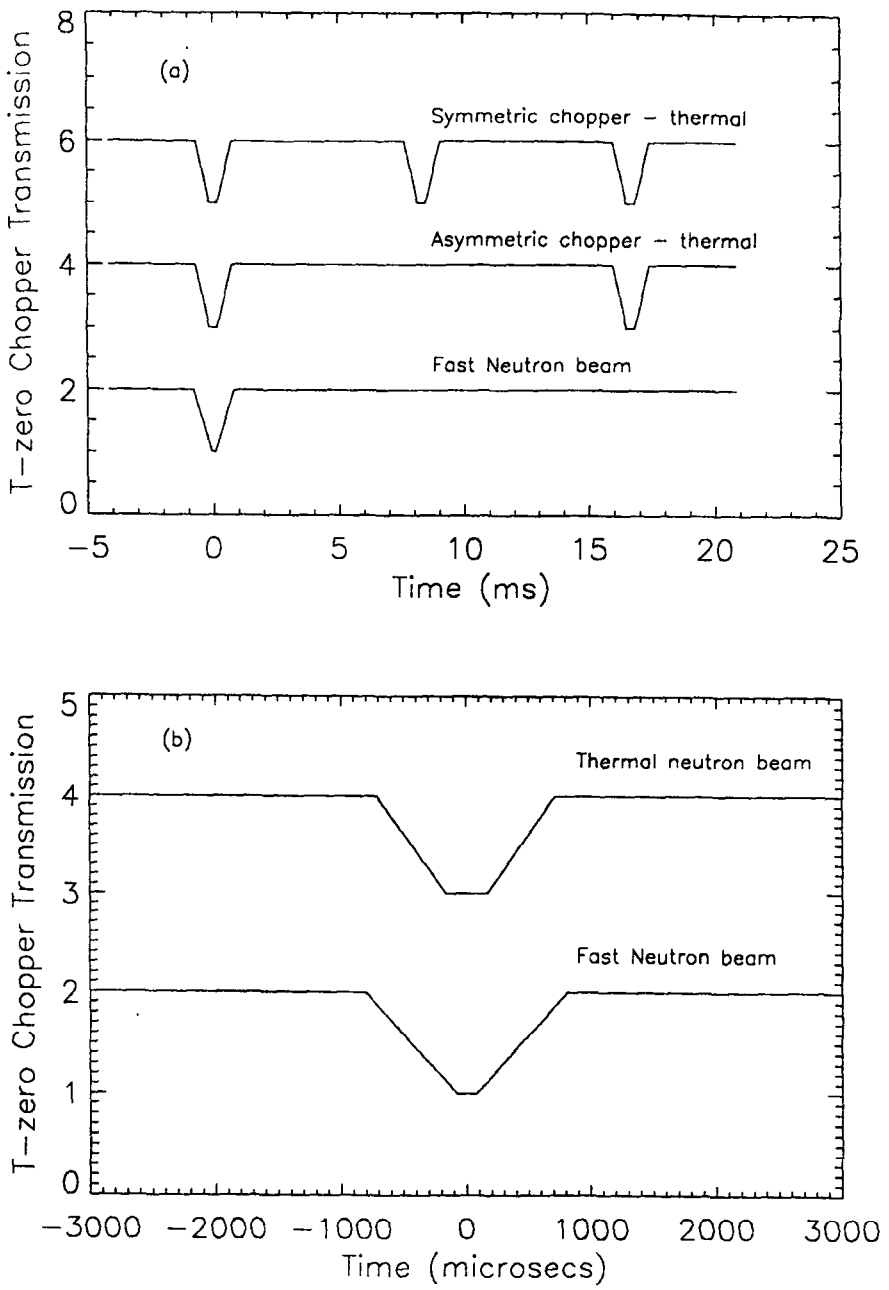

Figure 7 Calculated neutron-beam transmissions for the PHAROS t-zero chopper (see Tables I and II, and/or Ref. 3, for parameters), assuming that the chopper is completely black and that the both the thermal and fast-neutron apertures are perfect absorbers. The real geometry has been approximated by one in which the edges of the chopper blade are radial from the shaft axis. In (a), the thermal-beam performance of the real symmetric chopper is shown, followed by an equivalent asymmetric chopper and the fast-neutron performance. In (b) the thermal and fast-neutron performance in the region close to t = 0 is shown. Note that the larger fast-neutron beam is fully closed for a shorter time than the thermal beam, in agreement with the values given in Table II.

$$E_{360}(\text{meV}) = 5.22697\times10^{-6}\left(\frac{L}{\nu}\right)^2 \qquad (10)$$

where E_{180} and E_{360} correspond to the symmetric and asymmetric cases respectively.

Of course, the chopper must work for every neutron pulse that the accelerator delivers, and it must therefore spin at a frequency which is an integer multiple of the accelerator frequency, for asymmetric rotors, or an integer multiple of half the accelerator frequency for symmetric rotors, as listed in Table I. Table II gives all of the relevant parameters for the PHAROS t-zero chopper, in addition to results from Equations (3) and (6-10)

For the future, there are number of assumptions that have been made in this very simple treatment. The first is that 30 cm of inconel is the "right" stopping length for this application. As far as I know, this question has not been studied in detail, beyond estimating the number of mean free paths in the MeV range. Using conservative approximations for the high-energy neutron cross sections of the constituent elements in inconel[4], 30 cm corresponds to 8.8 mean free paths, or an attenuation to 0.015% of the incident fast-neutron flux. This might be a fruitful area for future study using Monte-Carlo simulations.

The second assumption is that there is a well-defined "fast-neutron" beam that is larger than the thermal beam, as shown in Fig. 4. It would be worthwhile to investigate what the fast-neutron beam profile looks like for both simple beams with apertures and for guides, using Monte-Carlo simulation. The question of possible streaming around the chopper, and matching it to the neighbouring apertures (which have penumbra effects), could also be investigated.

It would also be worthwhile to investigate whether it is beneficial to include any other materials, like hydrogenous materials or thermal-neutron absorbers such as boron, cadmium or gadolinium, into the rotor or its surfaces.

Finally, it seems that the actual performance of such choppers has never been measured, and it would be desirable to do so in an experiment with detectors placed before and after the rotor.

ACKNOWLEDGEMENTS

I am grateful for discussion with Mark Taylor and Ben Etuk regarding the mechanical engineering aspects discussed here, and to Phil Seeger and Luc Daemen for useful discussion. This work was supported in part by the division of Basic Energy Sciences of the U.S. Department of Energy under contract number W-7405-ENG-36.

REFERENCES

1. "Neutron Scattering Instruments at the SNS - A Guide for Potential Users", Rutherford Appleton Laboratory, February 1985

2. see for instance the MARI spectrometer in "Experimental Facilities at ISIS", RAL-88-030, February 1988

3. R. A. Robinson, M. Nutter, R. L. Ricketts, E. Larson, J. P. Sandoval, P. Lysaght and B. J. Olivier, in proceedings of ICANS-XII, Abingdon, U.K., 24-28 May 1993, Rutherford Appleton Laboratory Report 94-025, Vol. I, p.44-51.

4. Inconel X-750 has nominal composition 73.0 wt.% Ni, 15.5 wt.% Cr, 7.0 wt.% Fe, 2.5 wt.% Ti, 1.0 wt. % Nb, 0.7 wt.% Al, 0.04 wt.% C. from ASM Metals Reference Book, 3rd Ed. (ASM International, Materials Park 1993) p. 383.

Table I: Parameters that affect t-zero chopper performance

	Constraints	Typical sensible values	Value for PHAROS
Material	mechanically strong strong fast-neutron scatterer high-Z material	Inconel, Nimonic, Be	Inconel X-750
Neutron path length through the material	> some number of fast-neutron mean free paths	not known	30 cm ~ 8.8 mean free paths
Rotation frequency, ν	n * ν_{source} (for asymmetric rotor) 0.5 * n * ν_{source} (for symmetric rotor)	10 < ν < 120 Hz	ν = 60 Hz (symmetric)
Width of blade, t	t > fast-neutron beam size (d_{fast})	10 < t < 500 mm	t = 116 mm
Radius of rotor, R	2 * t < R < 0.5 * distance to adjacent beam	100 < R < 1000 mm	R = 0.35 m
Source-Rotor distance, L	beyond biological shield, but before sample	5 < L < 20 m	L = 14 m

Table II: Parameters and Characterisics for the t-zero chopper on PHAROS[3] at LANSCE.

Parameter	Symbol	Standard/Thermal	Fast-Neutron
source-chopper distance	L	14 m	
chopper radius	R	350 mm	
chopper rotation frequency	ν	60 Hz	
chopper tip speed	v	132 ms^{-1}	
beam width	d	72.5 mm	96.9 mm
chopper blade width	t	116.0 mm	
Idealised maximum energy	E_{max}	3.39 eV	1.90 eV
Energy at which beam begins opening	E_{start}	37.7 eV	195 eV
Energy at which beam is fully open	E_{full}	1.86 eV	1.47 eV
Energy when other blade re-enters beam	E_{180}	14.75 meV (12.5 - 17.6 meV)	
Energy when original blade re-enters beam	E_{360}	3.69 meV (3.4 - 4.0 meV)	
allowable jitter	t_{jitter} (μs)	165 μs	72.4 μs